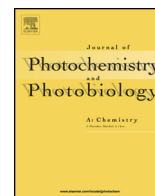




Contents lists available at ScienceDirect

# Journal of Photochemistry and Photobiology A: Chemistry

journal homepage: [www.elsevier.com/locate/jphotochem](http://www.elsevier.com/locate/jphotochem)

## Influence of poly(vinyl alcohol) on cellulose photochemical stability in cryogels during UV irradiation



Cristian-Drăgăș Varganici, Liliana Rosu, Oana Maria Mocanu (Paduraru), Dan Rosu\*

Centre of Advanced Research in Bionanoconjugates and Biopolymers, "Petru Poni" Institute of Macromolecular Chemistry, 41A Gr. Ghica-Voda Alley, 700487 Iasi, Romania

## ARTICLE INFO

## Article history:

Received 10 July 2014

Received in revised form 30 September 2014

Accepted 4 October 2014

Available online 17 October 2014

**Paper dedicated to the 65th anniversary of "Petru Poni" Institute of Macromolecular Chemistry of Romanian Academy, Iasi, Romania.**

## Keywords:

Photochemical behavior

Cellulose

Cryogels

Poly(vinyl alcohol)

Color analysis

FTIR

## ABSTRACT

The paper deals with surface properties modifications of cryogels based on poly(vinyl alcohol) and cellulose during exposure to several doses of ultraviolet (UV) irradiation. Significant color changes were observed during UV exposure. The cryogels exhibited a fading trend with irradiation dose increase. Structures accumulated instable red chromophores and exhibited a yellowing tendency. The ultraviolet-visible (UV-vis), X-ray photoelectron spectroscopy (XPS) and Fourier transform infrared (FTIR) spectra indicated important structural modifications during irradiation. The cryogels followed a complex photodecomposition mechanism through random macromolecular chain scissions accompanied by decarbonylation and photooxidation with carbonyl and carboxyl groups accumulation. Hydroperoxides, which were confirmed by an iodometric method, acted as important initiating sites. Cellulose chains were photochemically protected by poly(vinyl alcohol) up to a concentration of 70% in the cryogels, after which phase separation phenomena occurred as demonstrated by scanning electron microscopy technique (SEM), thus ending the protective effect of PVA. The major evolved volatile compounds during cryogels photodecomposition were identified by means of mass spectrometry (MS) and were the following: acetic acid, acetone, 2-propenal, propanoic acid, butanoic acid and ethyl methyl ketone.

© 2014 Elsevier B.V. All rights reserved.

### 1. Introduction

Cryogels are three-dimensional physically or chemically cross-linked polymer networks formed in frozen solutions of polymeric or monomeric precursors which are capable of absorbing high quantities of water and biological fluids, allowing safe diffusion of solutes and mass transport of nano- and microparticles. In addition, polymeric cryogels are excellent carriers designed for immobilization of different cells and biomolecules [1,2]. In contrast to chemically crosslinked hydrogels, the physically crosslinked ones exhibit increased strength due to their crystalline regions and possess superior elasticity [3,4].

Poly(vinyl alcohol) (PVA) has a strong hydrogen bonding capacity, is water soluble, biocompatible and biodegradable, thus being a good material for obtaining blends with natural polymers [5]. Natural polymers are used due to their wide properties range and also from ecological and economical perspectives. PVA cryogels encompass a wide palette of applications including

membranes for biosensors, drug and aroma controlled release carriers, scaffolds in tissue engineering, biodegradable packaging materials in food industry, etc. [6–11]. PVA and polysaccharides based cryogels are reported as good candidates for wound dressings, creating appropriate conditions for healing processes whilst assuring a shield against infections [12,13]. A moist environment promotes wound healing enhancement, making PVA/polysaccharides hydrogels suitable as dressings for such purposes, by assuring an appropriate moisture level at the wound-dressing interface. Such materials possess exudates absorbance capacities, are excellent wound desiccation retardants and non-adhesive, may incorporate and deliver bioactive principles and assure a barrier against microorganisms. Paduraru et al. [14] synthesized PVA/cellulose cryogels, which make the subject of the present study, and tested them "in vitro" as carriers for the delivery of vanillin, which is an antioxidant and antimicrobial agent. The strength and the swelling performances of these cryogels were improved by the cellulose content. Also, the increased cellulose content in the cryogels enhanced the released percentage of vanillin from their structures and shortened the half time and maximum release time. Varganici et al. reported a pyrolysis study on the same structures [15]. Decomposition studies in different

\* Corresponding author. Tel.: +40 232 217 454; fax: +40 232 211 299.  
E-mail addresses: [drosu@icmpp.ro](mailto:drosu@icmpp.ro), [dan\\_rosu50@yahoo.com](mailto:dan_rosu50@yahoo.com) (D. Rosu).

conditions of pure cellulose and PVA have been published [16,17]. However, no literature studies have been reported on the photochemical behavior of PVA/cellulose cryogels. UV radiation may cause significant changes in polymer structure influencing both the physico-mechanical strength as well as the surface properties [18–20]. The scission of macromolecular chains, cross-linking, branching, oxidation and loss of side groups are the main effects of the UV radiation action on organic polymers.

Because UV radiation induces damages to materials containing polymers and modifies their surface properties, the investigation of photochemical reactions that occur in complex polymer systems shows a great practical importance [21]. UV irradiation may also be used for surface properties modification, thus knowledge on the photochemical decomposition mechanism must be accumulated.

The aim of this paper is to study the UV radiation induced reactions on PVA/cellulose cryogels and to explain the stabilization effect between the two components of the cryogels with establishment of photodecomposition mechanisms.

## 2. Materials and methods

### 2.1. Materials

Microcrystalline cellulose Avicel PH-101 was obtained from Fluka. PVA with an average molecular weight of 147,000–186,000 and a hydrolysis degree of 99% was purchased from Aldrich.

### 2.2. Synthesis

Three cryogels were obtained with PVA as scaffold and increasing cellulose content, according to Table 1. The cryogels synthesis and structural characterization was described in a previous paper [14].

### 2.3. Irradiation

30 mm<sup>2</sup> (6 × 5 mm) of samples, 100 ± 2 μm thick, were irradiated with a medium pressure OSRAM HQE-40 lamp, as artificial light source and in the range 240–400 nm with a power of 100 W. Irradiation of the samples was performed in air. A rotating hexagonal prism shaped device, as sample carrier, with the light source positioned on the central axis of the prism was used. Structures were protected from thermal degradation using a distilled water filter and a fan. Radiations with λ < 300 nm, absent in the natural light spectrum, were hindered with an incorporated quartz/borosilicate filter having a maximum transparency at 365 nm. The irradiance value, measured at a distance of 60 mm from the source was 9.7 mW cm<sup>-2</sup>. This value was about 4.4 times higher than the average UV irradiance measured outdoors at zenith on a clear summer day (2.2 mW cm<sup>-2</sup>), which is lower than the medium value in Japan (3.5 mW cm<sup>-2</sup>) [22]. Measurements of irradiance and of radiance exposure, dependent on the irradiation time, were carried out with a PMA 2100 radiometer provided with a UVA detector, type PMA 2110 (Solar Light Co., USA). The temperature inside of the irradiation device was 20–22 °C. The

relative air humidity (RH) was varied between 50% and 55%. The temperature and RH values during irradiation were controlled with a thermo-hygrometer model JK-HTM-3 (Shanghai Jingke Scientific Instrument Co., China). The structures were removed from the irradiation device every 20 h and analysed.

### 2.4. Analytical methods

Samples thickness was measured with a PosiTector 200 instrument from Defelsko USA. Color analyses were conducted with a PocketSpec apparatus purchased from Color QA SUA having a sensor head of 6 mm in diameter. The device was calibrated with a super white sulphate barium pellet. Measurements were conducted under reflectance mode using D<sub>65</sub> illuminant at 10° standard observer. Results were extracted in the CIELAB system. The color parameters of this system are the following: the L\* axis is the lightness (ranging from 0 (black) to 100 (white)), whilst a\* and b\* axes represent the chromaticity coordinates (a positive a\* value corresponding to red and a negative a\* value to green, whilst +b\* and -b\* denote yellow and blue, respectively). The FTIR spectra were recorded using a Bruker Vertex 70 device equipped with a MIRacle accessory designed for single or multi-reflection attenuated total reflectance (ATR). The ATR crystal plate was made from diamond and the solid material was put in physical contact with the sampling area through high pressure clamping in order to record high-quality and reproducible spectra. The spectra were recorded in the range 4000–600 cm<sup>-1</sup> at a spectral resolution of 4 cm<sup>-1</sup> and 64 scans. FTIR spectra signals were assigned using the literature data [23]. The FTIR spectra were recorded in mostly the same point of each same sample. In order to eliminate eventual thickness variation errors during photoirradiation, normalization of spectra was conducted. This was done through dividing the whole spectrum surface by sample thickness after each irradiation time, which is a common procedure in such cases. Changes in UV-vis spectra were monitored with a SPECORD 200 Analytik Jena spectrophotometer equipped with an integrated Industries sphere. The device was used in reflectance mode. Spectra were recorded in the range 400–800 nm and samples were used as non-transparent pellets, except PVA which was used as film. X-ray photoelectron spectroscopy (XPS) experiments were performed on a KRATOS Axis Nova (Kratos Analytical, Manchester, UK) spectrometer, using a monochromatic AlKα source (1486.6 eV), with 10 mA current and 15 kV, and base pressure of 10<sup>-8</sup>–10<sup>-9</sup> Torr in the sample chamber. The incident mono-chromic X-ray beam was focused on a 0.7 × 0.3 mm<sup>2</sup> area of the surface. The XPS survey spectra of the samples were collected in the range of -10 to 1200 eV with a resolution of 1 eV and a pass energy of 160 eV. The high-resolution spectra for all the elements identified from the survey spectra were collected using pass energy of 20 eV and a step size of 0.1 eV. The binding energy of the C<sub>1s</sub> peak was normalized to 285 eV. To determine the type of O–C bonds present, a chemical bond analysis of carbon was accomplished by the deconvolution of the curve into corresponding peaks. Data were analyzed using the Vision software from Kratos (Vision 2.2.10). Scanning electron micrographs were taken on liquid nitrogen fractured samples, with a Quanta 200 instrument. The fractured surface was coated with a gold layer. Hydroperoxides determination was undertaken by applying an iodometric method described in the literature [24]. According to the method 0.1 g of irradiated sample was immersed in 15 mL chloroform in a round bottom flask in nitrogen atmosphere. To this solution was added a 10 mL mixture of acetic acid:chloroform (2:1). 1 mL potassium iodide solution was added to the mixture after 10 min. The flask was sealed after 2 min and left in the dark for 1 h under stirring. Hydroperoxide concentration was determined by measuring the absorbance at 362 nm with the help of a calibration curve obtained from known quantities of

**Table 1**  
Cryogels composition.

Sample code	Composition (%)	
	PVA	Cellulose
PVA	100	0
90/10	90	10
70/30	70	30
50/50	50	50
Cellulose	0	100

hydroperoxide. The evolved volatile compounds analyses were performed with a TGA–MS system. The system was equipped with an apparatus of simultaneous TGA/DSC analyses STA 449F1 Jupiter model (Netzsch, Germany) and a mass spectrometer QMS 403C Aeolos model (Netzsch, Germany). The TG/DSC thermobalance was coupled online with mass spectrometer through one heated transfer line. 50 mg of samples were heated under nitrogen flow (flow rate  $50 \text{ mL min}^{-1}$ ), on an  $\text{Al}_2\text{O}_3$  plate with a  $30^\circ\text{C min}^{-1}$  heating rate starting from room temperature. For the determination of the volatile compounds from the 260 h UV irradiated PVA and 70/30 cryogel, the heating was done up to  $50^\circ\text{C}$  below the onset temperatures of thermal decomposition ( $217^\circ\text{C}$  for pure PVA and  $198^\circ\text{C}$  for 70/30 cryogel [14]). Isothermals were kept at the certain temperatures ( $150^\circ\text{C}$  for PVA and  $170^\circ\text{C}$  for 70/30 cryogel) for 2 h. The evolved volatile mixture from the photodecomposed products was moved by nitrogen through the MS transfer line. The transfer line to MS spectrometer QMS 403C was made of a quartz capillary with an internal diameter of  $75 \mu\text{m}$  and was heated at  $190^\circ\text{C}$ . The mass spectra were recorded under electron ionization energy of 70 eV. Data were scanned in the range  $m/z = 1\text{--}300$ . The NIST Mass Spectral Database was used for the identification of ion fragments ( $m/z$ ) in MS spectra. The volatile products were identified by means of mass spectra and signal ratios.

### 3. Results and discussions

#### 3.1. Color modification studies

To our knowledge, no study has focused on the color modifications in the CIELAB system during UV irradiation of cellulose and PVA based cryogels.

Significant color changes were found during irradiation. A fading trend of samples with increase of irradiation dose was observed. Fig. 1 shows that the lightness factor ( $L^*$ ) increases with irradiation dose.

The most important changes in  $L^*$  values were recorded for cellulose ( $\Delta L^* = 14.99$ ) and PVA ( $\Delta L^* = 10.54$ ) at the highest irradiation dose value ( $1266 \text{ J cm}^{-2}$ ). A slow variation of  $L^*$  was recorded up to  $584 \text{ J cm}^{-2}$  irradiation dose, or 120 h irradiation time, respectively, for both polymers which indicated the presence

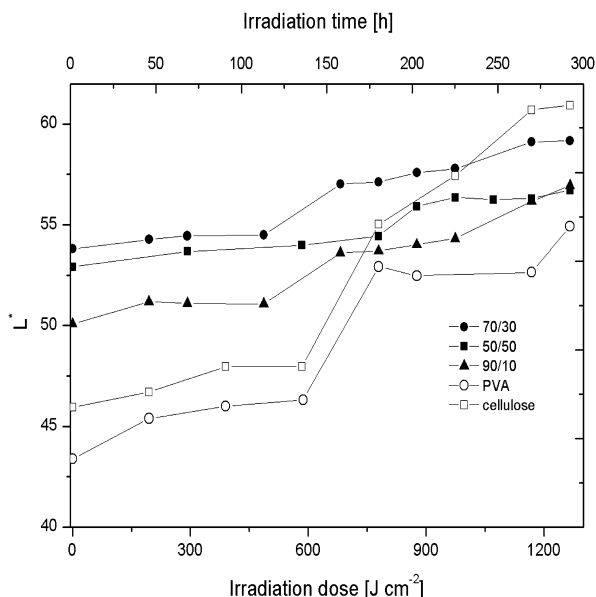


Fig. 1. Variation of lightness factor with irradiation dose.

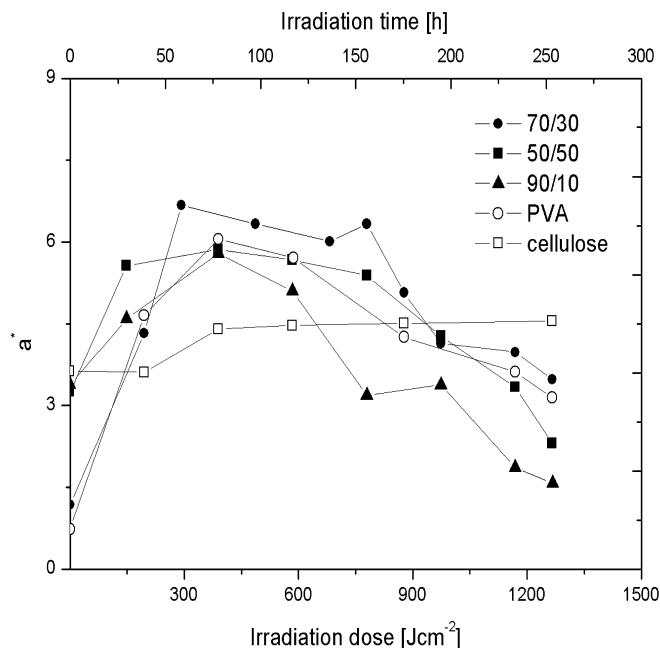


Fig. 2. Variation of chromatic coefficient  $a^*$  with irradiation time.

of an induction time or of a critical dose of irradiation. As soon as the induction period or the critical irradiation dose was exceeded, a sharp increase of  $L^*$  occurred. The variations of  $L^*$  values with irradiation dose for PVA/cellulose blends were much lower than for the starting polymers.  $\Delta L^*$  values recorded at maximum irradiation dose values for each sample decreased with the increasing of cellulose content in the mixture.

Figs. 2 and 3 show the variation of the chromatic coefficients  $a^*$  and  $b^*$  during irradiation.

It can be observed from Fig. 2 that pure cellulose exhibits a slow increase in  $a^*$  values in the range  $195\text{--}390 \text{ J cm}^{-2}$  irradiation dose ( $40\text{--}80 \text{ h}$  irradiation time) due to small amounts of red chromophores accumulated on the surface. After the accumulation of

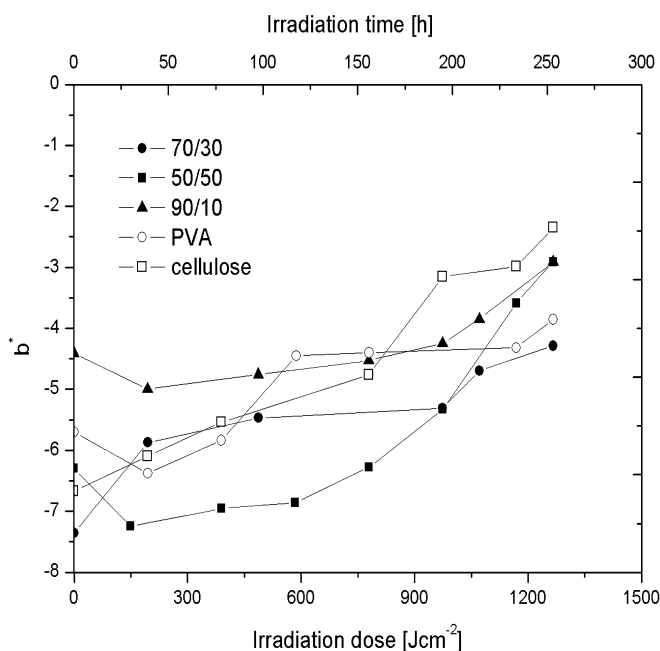


Fig. 3. Variation of chromatic coefficient  $b^*$  with irradiation time.

these chromophores, cellulose exhibits a stable plateau for  $a^*$  values after an irradiation dose value of  $390 \text{ J cm}^{-2}$  (80 h irradiation time). The  $b^*$  values (Fig. 3) variation shows the tendency of yellowing of pure cellulose during the whole irradiation process due to the continuous accumulation of yellow chromophore compounds. Similar results were found by Yatagai and Zeronian [25] who reported that  $\Delta E$  values increased by formation of chromophore groups consisting of conjugated unsaturated structures and carboxyl entities which led to surface yellowing during UV exposure. Fig. 2 shows that, unlike cellulose, pure PVA exhibits a different photochemical behavior. This aspect can also be noticed for all the cryogels which exhibit the same trend. The photochemical behavior trend can be divided in two stages. The former stage, up to 80 h ( $390 \text{ J cm}^{-2}$  irradiation dose), consists in a fast accumulation of instable red chromophores which start decomposing in the latter stage. Fig. 3 shows a continuous increase of  $b^*$  with irradiation dose of PVA, due to surface yellowing. Similar results for poly(vinyl chloride) were reported in the literature [26,27].

### 3.2. UV-vis spectroscopy

Fig. 4a shows the reflectance spectra of PVA and cellulose. It can be observed from Fig. 4a an increase in reflectance with

irradiation time and dose. This aspect is in a good agreement with the colorimetric studies which showed a high increase of  $L^*$  values, whiter surfaces being capable of a higher light reflecting capacity. This higher light reflecting capacity proved to be superior to the effect of variation of chromatic coordinates  $a^*$  and  $b^*$  during irradiation in these cases.

In the case of the 70/30 cryogel one can observe a decrease in reflectance with irradiation time and dose increase (Fig. 4b). This aspect is in good agreement with the  $L^*$  values which show a lower increase with irradiation time and dose. However, in the case of cryogels the variations of chromatic coefficients  $a^*$  and  $b^*$  are comparable to the variations of  $L^*$  values, this being reflected in a significant influence on the reflectance. The chromophores generated during UV irradiation absorb light in the range 500–800 nm, thus leading to a decrease in reflectance values, aspect which may be correlated to yellowing of the cryogels surfaces, equivalent to an increase in  $b^*$  values [28].

### 3.3. Structural characterization by FTIR

Fig. 5 depicts the FTIR spectra before irradiation, after 260 h irradiation time ( $1266 \text{ J cm}^{-2}$  irradiation dose) and the difference spectrum for the pure PVA (Fig. 5a), cellulose (Fig. 5b) and sample 70/30 (Fig. 5c). As an exemplification, structure 70/30 was

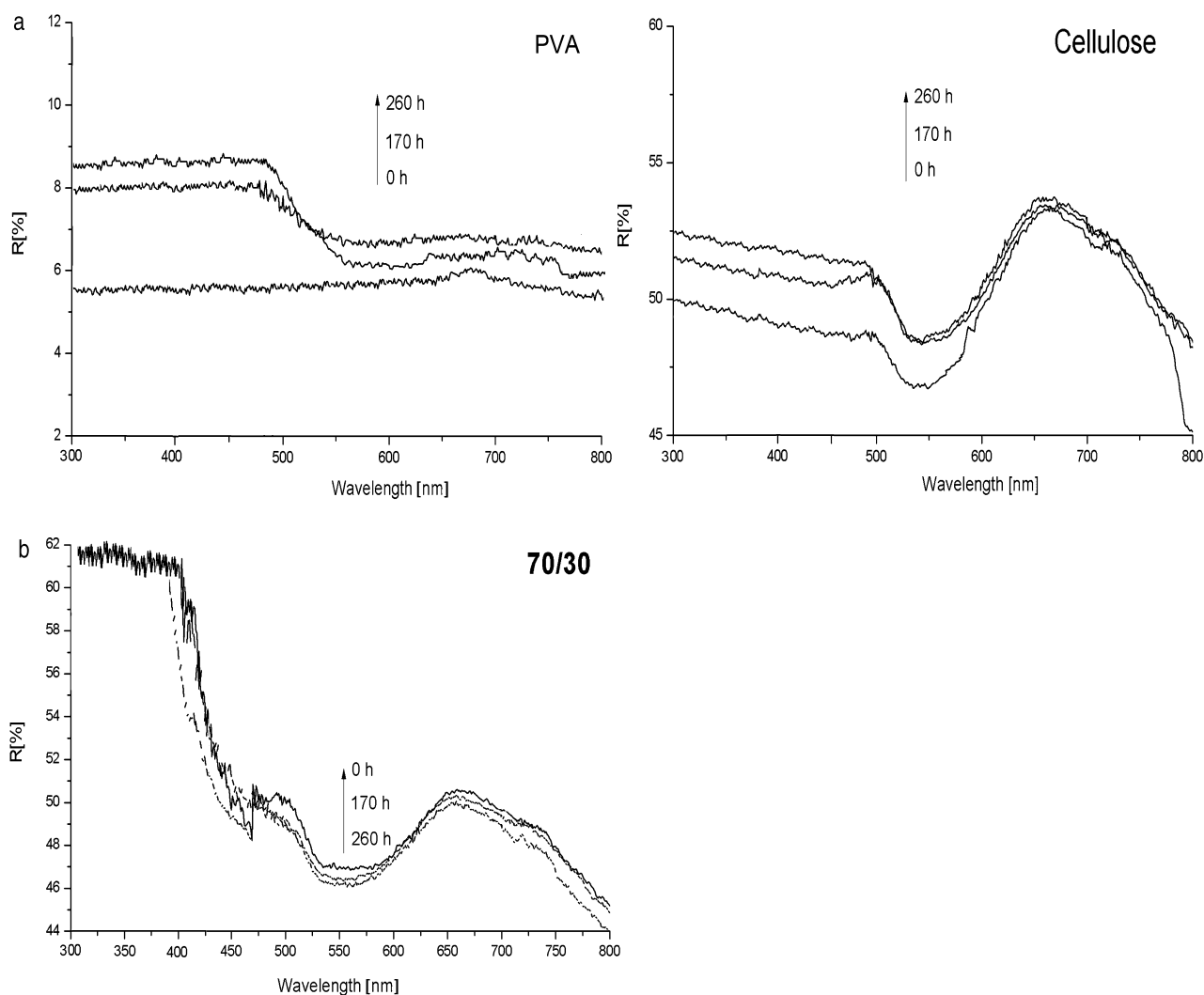
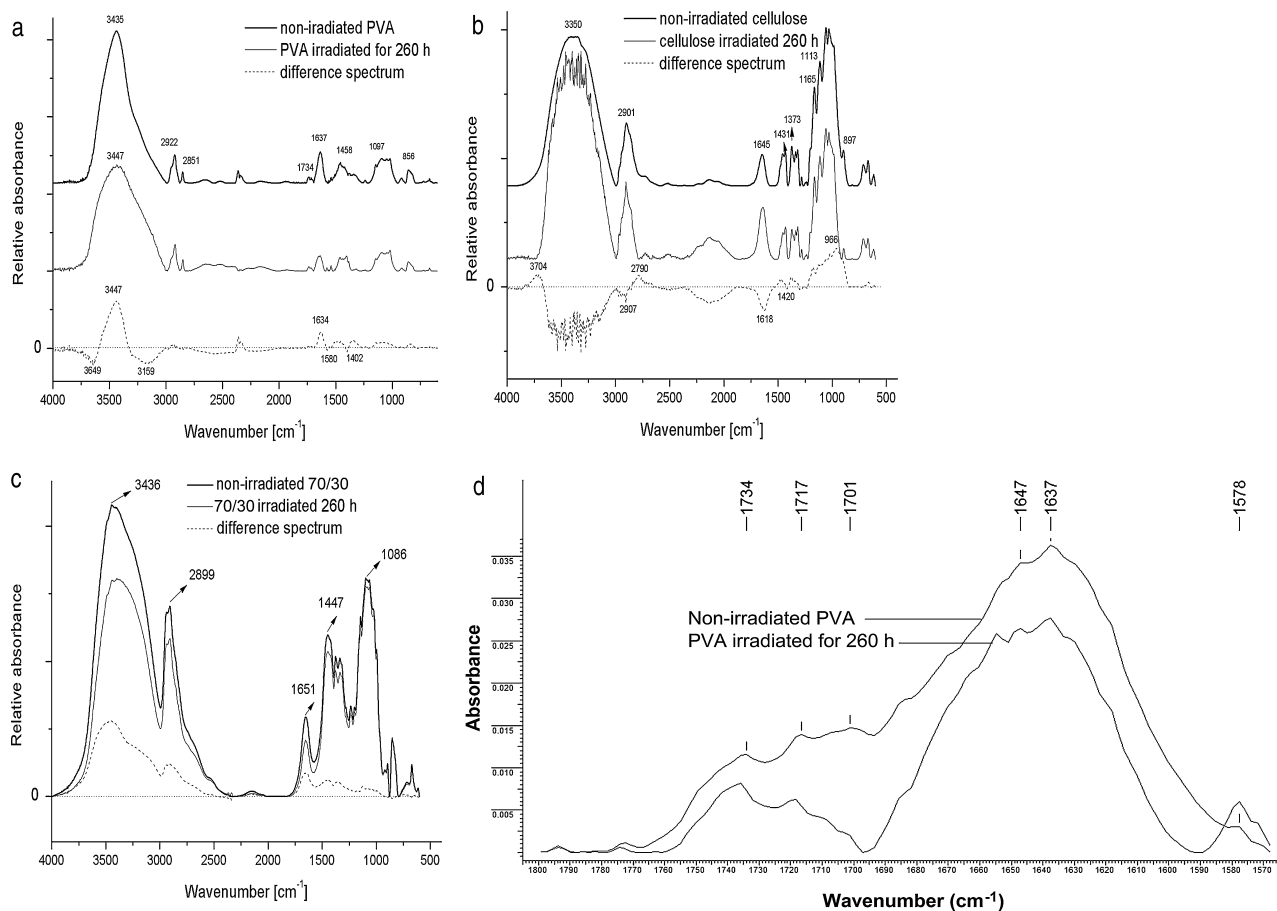


Fig. 4. (a) Reflectance spectra of PVA and cellulose and (b) reflectance spectra of cryogel 70/30.



**Fig. 5.** (a) FTIR spectra of PVA, (b) FTIR spectra of cellulose, (c) FTIR spectra of cryogel 70/30, and (d) carbonyl region in the FTIR spectrum of non-irradiated PVA and PVA after 260 h irradiation time.

aken into account, due to the other cryogels similar photochemical behavior. Table 2 lists the main spectral features of the non-irradiated PVA and cellulose samples used in the study.

It can be observed that the FTIR spectrum of sample 70/30 (Fig. 5c) contains absorption bands of both comprising polymers. Furthermore, both constituents of the cryogels exhibit absorption bands specific to carbonyl groups (Fig. 5a and b), which are

**Table 2**  
Assignments of the main FTIR signals of non-irradiated PVA and cellulose.

PVA		
Wavenumbers (cm <sup>-1</sup> )	Assignments	References
2800–3000	CH <sub>3</sub> /CH <sub>2</sub> /CH stretching and deformation vibrations	[29]
1300–1500		
1458		
3000–3750	OH stretching	
3435		
1600–1800	Impurities and the presence of carbonyl entities from incomplete saponification or oxidation during preparation and processing	[21,30]
1637		
1734		
Cellulose		
Wavenumbers (cm <sup>-1</sup> )	Assignments	References
3000–3900	OH stretching	
3350		
2901	C–H stretching	
1431	Symmetric CH <sub>2</sub> bending (crystallinity band)	[31,32]
1645	Absorbed water and/or the oxydated hydroxy methylene group in the glucose units during industrial obtaining	[33]
1373	Symmetric C–H deformation	
1165	C–O–C asymmetric vibration	
897–1113	Asymmetric glucose ring and C–O stretching	[33]
897	β-(1→4)-Glycosidic bonds stretching (amorphous state band)	[31,32]



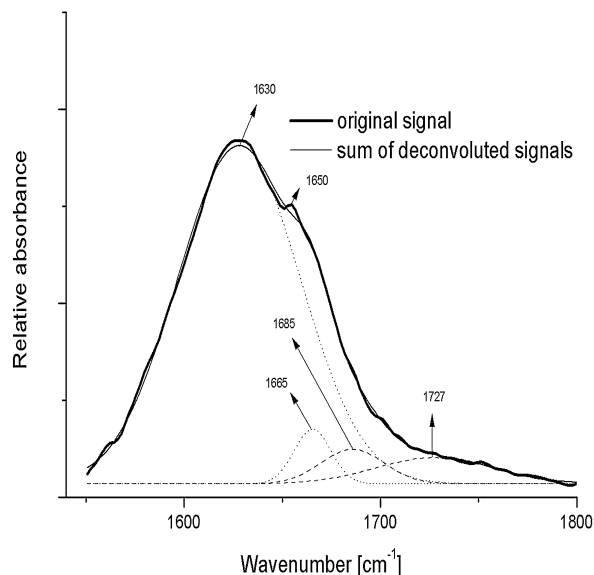


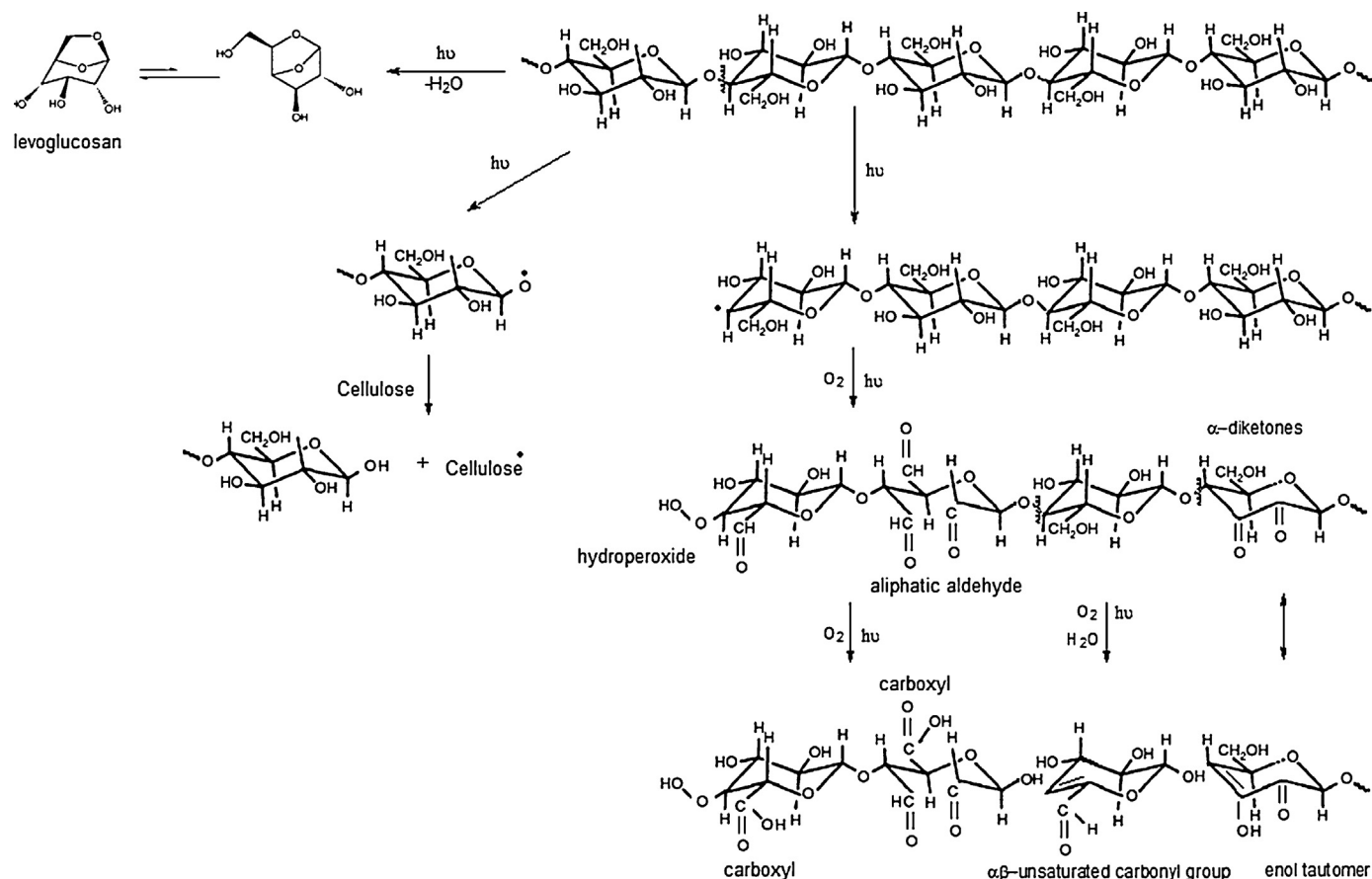
**Fig. 6.** Deconvoluted peaks in the range 1500–1800  $\text{cm}^{-1}$  for photodegraded cellulose.

remaining acetate groups during PVA backbone photocleavage, explained by the lowering in intensity of the carbonyl region [37,38]. Also the impurities and/or oxidation products formed during preparation and processing may represent important initiating sites for photooxidation [30]. The new peak at 1578  $\text{cm}^{-1}$ , in Fig. 5d, which is significantly intense and broader

for the irradiated PVA, corresponds to the C–H stretching vibration adjacent to C=C bonds newly generated unsaturated structures resulted during photoirradiation. This peak confirms the correct attribution of the peak at 1580  $\text{cm}^{-1}$  in the difference spectrum in Fig. 5a, to C=C unsaturated structures. The peak at 1734  $\text{cm}^{-1}$  corresponds to the acetate moieties [28] and/or oxidation during preparation and processing in the non-irradiated PVA spectrum [21,30]. Its lowering in intensity in the spectrum of the PVA irradiated for 260 h is attributed to the cleavage of acetate moieties which generate acetic acid through Norrish II reactions. The peak at 1701  $\text{cm}^{-1}$  had considerably lowered in intensity in the spectrum of the PVA irradiated for 260 h. This aspect was explained by the formation of unsaturated aldehyde entities during photoirradiation [28].

The difference FTIR spectrum of cellulose (Fig. 5b) indicates the occurring of intense photooxidation processes during irradiation. The broad signal containing multiple peaks in the range 3150–3623  $\text{cm}^{-1}$  corresponds to the formation of new hydroperoxidic structures [39]. The new broad peak in the range 1522–1837  $\text{cm}^{-1}$  confirms the occurrence of photooxidation processes via the formation of new carbonyl structures [23]. By applying the second derivative a deconvolution was possible, leading to the identification of four previously overlapped signals with peak values at 1630  $\text{cm}^{-1}$ , 1665  $\text{cm}^{-1}$ , 1685  $\text{cm}^{-1}$  and 1727  $\text{cm}^{-1}$ , as it can be observed in Fig. 6.

The signal at 1630  $\text{cm}^{-1}$  is attributed to the formation of some C=C bonds possibly conjugated with other double bonds or carbonyl and/or carboxyl groups resulted during cellulose photodegradation [23]. The peak at 1665  $\text{cm}^{-1}$  is attributed to C<sub>2</sub>–C<sub>3</sub>  $\alpha$ -diketones formation which may undergo keto–enol tautomerism. These diketones are responsible for cellulose yellowing and



**Scheme 2.** Proposed photodecomposition mechanism of cellulose.

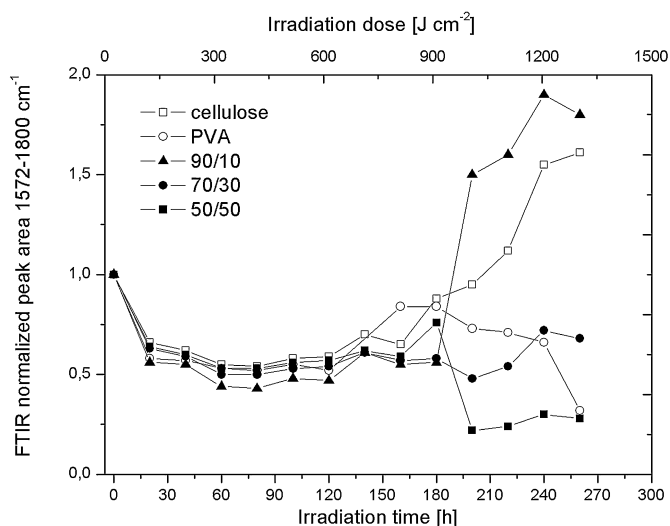


**Fig. 7.** Variation of carbonyl normalized peak area values with irradiation time and dose.

their formation occurs regardless of hydrolysis phenomena in the main cellulose backbone [40]. From Fig. 6 there can also be observed a weak signal at  $1650\text{ cm}^{-1}$  attributed to C=C stretching vibration which is often masked by the water absorption band at the same frequency [40]. The signal at  $1685\text{ cm}^{-1}$  corresponds to photooxidation of  $\text{C}_6$  from cellulose structure which, together with internal dehydration, generates  $\alpha\beta$ -unsaturated aldehydes, again with the peak at  $1650\text{ cm}^{-1}$ . Further photocleavage of the cellulose  $\text{C}_2\text{--C}_3$  bonds leads to conjugated unsaturated structures which are further lost during irradiation, this being a specific photoreaction of cellulose under sunlight exposure [40]. In this sense, the signal peak at  $1727\text{ cm}^{-1}$  may correspond to aliphatic aldehyde structures [39]. In Fig. 5b, the decrease in the signals in the region  $1113\text{--}897\text{ cm}^{-1}$  with a peak at  $966\text{ cm}^{-1}$  in the difference spectrum may be attributed to cellulose depolymerization by glycosidic bonds cleavage. The decrease in absorption bands with peak values at  $2790\text{ cm}^{-1}$  and  $3704\text{ cm}^{-1}$  may correspond to some dehydration along with the formation of C=C bonds. The results found regarding the photodegradation of the individual cellulosic component are in good agreement with other literature data, according to which photooxidative processes lead to an increase in carboxyl, carbonyl and hydroperoxide groups and a significant lowering of polymerization degree. These photochemical transformations are in concordance with the discussed modifications in color parameters. Desai and Shields [41] showed that cellulose

**Table 3**  
Summary of  $\text{C}_{1s}$  peak deconvolutions (%).

Compound	BE (eV)	Assignment	0 h	260 h
Cellulose	285	C–C and C–H	14.24	16.02
	286.6	C–O	66.76	63.62
	288	O–C–O	19	17.57
	298.1	C=O	–	2.79
PVA	285	C–C and C–H	74.71	68.39
	286.4	C–O	20.10	23.23
	287.7	C=O	3.05	4.69
	289.2	O–C=O	2.14	3.69
70/30	285	C–C and C–H	54.89	48.84
	286.4	C–O	38.12	42.80
	287.6	C=O	4.31	6.78
	288.5	O–C=O	2.59	1.58

photodegradation follows a random first order kinetic mechanism. The authors used gas chromatography for the identification of volatile products and found a mixture of methyl formate, acetaldehyde, acetone, propionaldehyde, methanol, ethanol, methane and ethane. The volatile mixture might have resulted from further degradation of intermediate glucose and oligosaccharides resulted from the initial chain cleavage process. A possible mechanism of cellulose photodecomposition is given in Scheme 2.

It can be observed from the difference spectrum in Fig. 5c that during photodegradation of sample 70/30 especially depolymerization processes occurred, as a final result of previous cleavage of intermediate instable products because the loss of functional groups does not lead to a decrease in intensity for all signals. Fig. 7 shows the variation of carbonyl normalized peak area values with irradiation time and dose. Normalizations were done by dividing the carbonyl area of the irradiated surface samples by the carbonyl area of the non-irradiated surface samples in FTIR.

Four stages can be observed from Fig. 7. The first stage (0–20 h) is represented by a sharp decrease of carbonyl content, due to macromolecular chain scissions accompanied by decarbonylation. The second stage (20–120 h) describes a slower decarbonylation process. In the third stage (120–180 h) photooxidation processes become more intense with carbonyl groups accumulation. In the last stage (180–260 h) the photodegradation processes continue either by photooxidation or decarbonylation as a function of cryogels composition. It can be observed from Fig. 7 that the carbonyl normalized peak area values, vary almost the same for all samples up to a  $900\text{ J cm}^{-2}$  irradiation dose value (180 h irradiation time), after which the sample containing 90% PVA exhibits intense photooxidation phenomena, similar to pure cellulose. Because of a

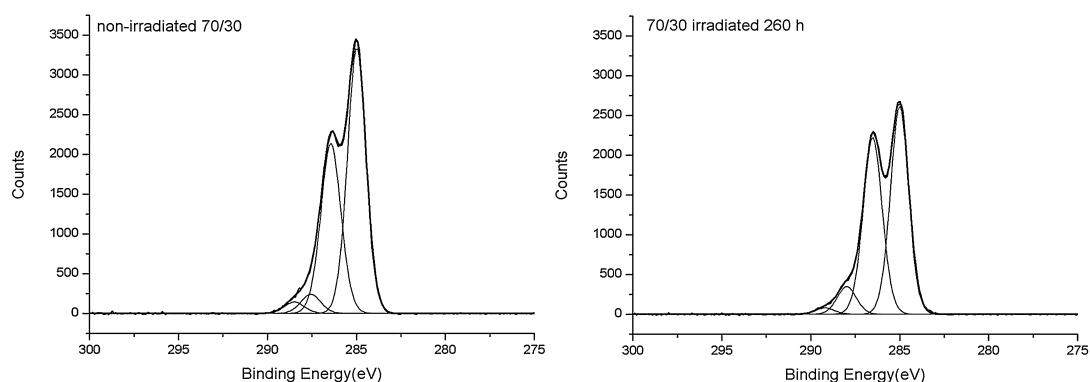


**Fig. 8.**  $\text{C}_{1s}$  fitted curves of cryogel 70/30 before and after 256 h of photooxidation.

**Table 4**

Volatile organic compounds evolved from irradiated PVA film identified by TG–MS analysis.

Main fragment <i>m/z</i>	Molecular weight (g mol <sup>-1</sup> )	Identification
60, 45, 43, 15	60	Acetic acid
58, 43, 42, 15	58	Acetone
56, 55, 29, 27	56	2-Propenal
74, 45, 29, 28	74	Propanoic acid
88, 73, 60, 41	88	Butanoic acid
72, 43, 29, 27	72	Ethyl methyl ketone

more compact structure, the pure PVA undergoes a slower photooxidation process, probably because of hardening of air diffusion in the polymer bulk. Due to this aspect, photooxidation occurs only at the surface by intermediate hydroperoxide formation. Unlike PVA, pure cellulose, which presents gaps between chains, exhibits photooxidation phenomena in bulk by continuous hydroperoxide formation. It can be observed that content up to 70% PVA protects the cellulose chains from photooxidation. At a 90% PVA concentration the photooxidation processes become very intense, probably due to phase separation phenomena occurrence, demonstrated by SEM technique in a previous paper, due to cellulose islands formation in the PVA matrix [14].

### 3.4. Structural analysis by XPS

XPS spectra of pure components and of 70/30 cryogel showed, as expected, carbon (C<sub>1s</sub> at 285 eV) and oxygen (O<sub>1s</sub> at 532 eV) atoms as the two major constituents. Fig. 8 displays the C<sub>1s</sub> deconvoluted peaks of sample 70/30 before and after 260 h irradiation time. The C<sub>1s</sub> deconvolution results of both comprising polymers and that of cryogel 70/30 before and after 260 h irradiation time are summarized in Table 3. The characteristic values of data in Table 3 were in good agreement with literature data for both PVA [36] and cellulose [42].

One may observe from Table 3 that photooxidation led to a decrease in C–C and C–H entities from 70/30 cryogel. This aspect is due to the oxidation of the alkyl chains. Also an increase in moieties containing C–O bonds may be noticed. The formation of new hydroperoxidic structures during photooxidation of 70/30 cryogel may explain this behavior. The oxidation of alkyl chains from the cryogels occurs simultaneously with continuous hydroperoxide formation. The increase in C=O bonds content may be explained by new carboxylic groups formation during photooxidation, as shown in Scheme 1. A significant decrease in O–C=O content, from residual acetate groups in PVA, after irradiation is due to the Norrish II reaction, leading to acetic acid formation. Oxygen fixation and formation of oxidized products lead to a slight increase of the O/C ratio in the cryogels after

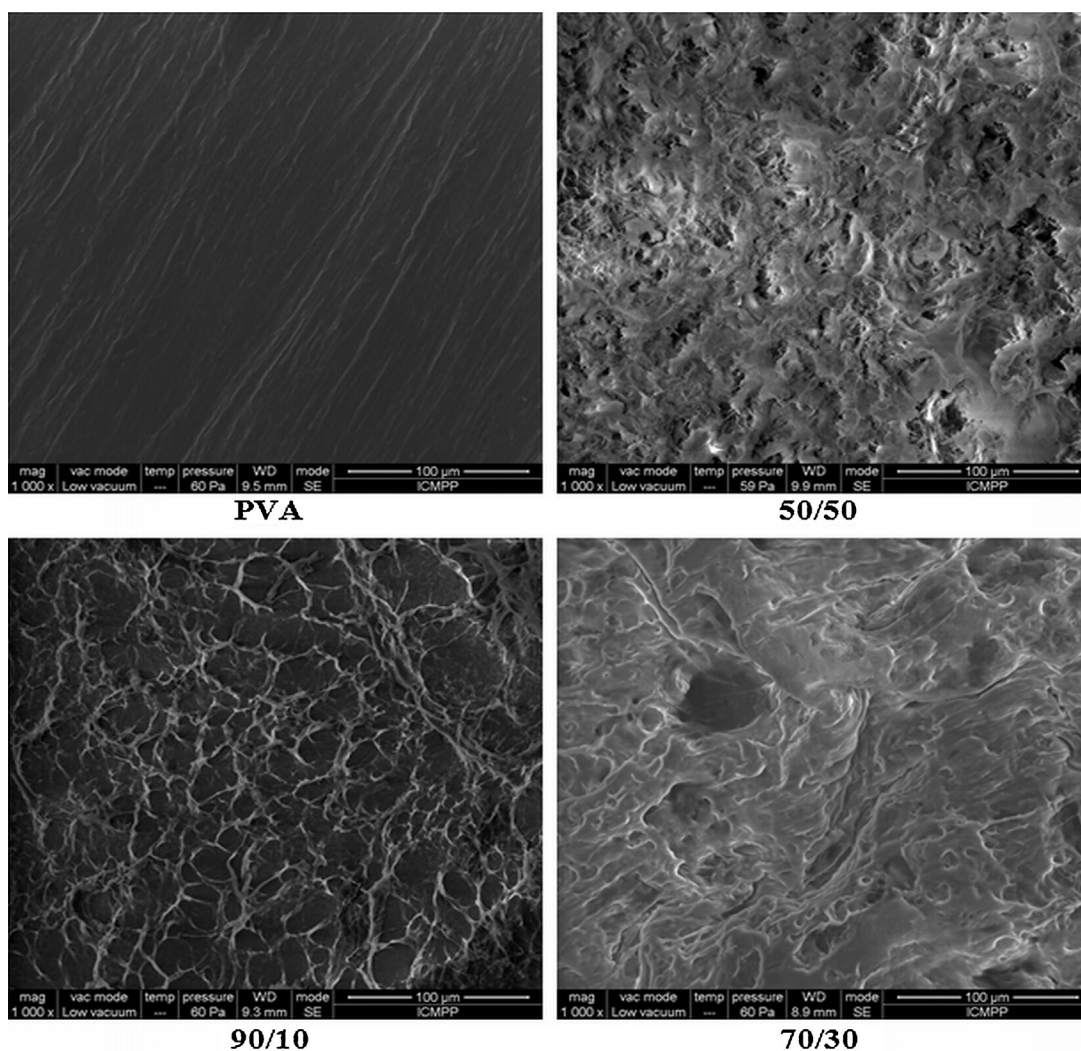


Fig. 9. SEM images of PVA and cryogels (magnification 1000×).

irradiation from 0.378 to 0.389. This aspect is in good agreement with Fig. 8, which shows that no new peaks were formed during irradiation, and with Fig. 5c in which the FTIR difference spectrum indicated no significant formation of photooxidative products. All the above mentioned aspects confirm that, up to a concentration of 70%, PVA retards cellulose photochemical decomposition, thus behaving as an oxygen barrier, as described in literature [36].

### 3.5. Evolved volatile compounds analysis

Analyzing the MS spectra of the 70/30 cryogel, the following most abundant volatile components were identified and given in Table 4. One may observe that these findings are in good agreement with the photodecomposition mechanism proposed for PVA [36].

### 3.6. SEM characterization

Fig. 9 shows the SEM images of pure PVA and the cryogels before photoirradiation. One can observe from Fig. 9 that PVA has a compact structure. Also the 50/50 and 70/30 cryogels behave as composite structures in which PVA is the matrix and the cellulose is the reinforcement material. This aspect is in good agreement with above shown aspects, thus confirming that a PVA concentration up to 70% protects the cellulosic fibers from photodegradation, behaving as a barrier against photooxidation. There may also be observed from Fig. 9 that islands of cellulose tend to appear in the polymer matrix with PVA content increase due to partial compatibility between components. At a concentration of 90% PVA in the cryogels there appear two distinct phases, one comprised of the cellulosic fibers and that of PVA. In this case, the cellulose fibers may be significantly affected by UV irradiation due to lack of protection from the PVA matrix, as shown in Fig. 7.

## 4. Conclusions

Cryogels based on poly(vinyl alcohol) and varying cellulose content were exposed to different UV irradiation doses. Color changes were monitored during irradiation which led to significant structural changes. The cryogels showed a discoloration tendency with irradiation dose increase, due to lightness factor and chromatic coefficients values increase. The samples accumulated instable red chromophores and exhibited a yellowing tendency. Structural modifications during the photodecomposition were monitored by FTIR, UV–vis and XPS techniques. The cryogels photochemically decomposed following a complex mechanism. PVA underwent a slower photooxidation process, due to hardening of air diffusion, thus photooxidation occurred at the PVA surface by intermediate hydroperoxide formation which were confirmed by an iodometric method. Pure cellulose exhibited photooxidation phenomena in bulk by continuous hydroperoxide formation and especially depolymerization, because of the gaps between chains. Due to these aspects, cellulose chains were protected from UV irradiation by a concentration of PVA up to 70%, possibly arranged as coating on cellulose fibers. The findings were confirmed by SEM method because after a PVA concentration higher than 70%, phase separation phenomena occurred. The major evolved volatile compounds during cryogels were: acetic acid, acetone, 2-propenal, propanoic acid, butanoic acid and ethyl methyl ketone, as identified by TGA–MS method.

## Acknowledgements

This work was supported by a grant of the Romanian National Authority for Scientific Research, CNCS-UEFISCDI – Project number PN-II-ID-PCE-2011-3-0187. Authors are grateful to Dr. Anton

Airinei and Ph.D. student Adina Coroaba of the “Petru Poni” Institute of Macromolecular Chemistry of Romanian Academy, Iasi, Romania for the UV–vis and XPS measurements.

## References

- [1] V.I. Lozinsky, I.Y. Galaev, F.M. Plieva, I.N. Savina, H. Jungvid, B. Mattiasson, Polymeric cryogels as promising materials of biotechnological interest, *Trends Biotechnol.* 21 (10) (2003) 445–451.
- [2] S. Gupta, J.W. Thomas, A. Sinha, Evolution of PVA gels prepared without crosslinking agents as a cell adhesive surface, *J. Mater. Sci. Mater. Med.* 22 (2011) 1763–1772.
- [3] B. Bolto, T. Tran, M. Hoang, Z. Xie, Crosslinked poly(vinyl alcohol) membranes, *Prog. Polym. Sci.* 34 (2009) 969–981.
- [4] C.M. Hassan, N.A. Peppas, Cellular PVA hydrogels produced by freeze/thawing, *J. Appl. Polym. Sci.* 76 (2000) 2075–2079.
- [5] S. Tripathi, G.K. Mehrotra, P.K. Dutta, Physicochemical and bioactivity of crosslinked chitosan-PVA film for food packaging applications, *Int. J. Biol. Macromol.* 45 (2009) 372–376.
- [6] S. Patachia, Chr. Friedrich, C. Florea, C. Croitoru, Study of the PVA hydrogel behaviour in 1-butyl-3-methylimidazolium tetrafluoroborate ionic liquid, *Express Polym. Lett.* 5 (2011) 197–207.
- [7] O.M. Paduraru, C. Vasile, S. Patachia, C. Grigoras, A.M. Oprea, Membranes based on poly(vinyl alcohol)/ $\beta$ -cyclodextrin blends, *Polimery* 55 (2010) 473–478.
- [8] R.H. Schmedlen, K.S. Masters, J.L. West, Photocrosslinkable polyvinyl alcohol hydrogels that can be modified with cell adhesion peptides for use in tissue engineering, *Biomaterials* 23 (2002) 4325–4332.
- [9] J. Lange, Y. Wyser, Recent innovations in barrier technologies for plastic packaging – a review, *Packag. Technol. Sci.* 16 (2003) 149–158.
- [10] C.M. Hassan, N.A. Peppas, Structure and applications of poly(vinyl alcohol) hydrogels produced by conventional crosslinking or by freezing–thawing methods, *Adv. Polym. Sci.* 153 (2000) 37–65.
- [11] Y.N. Martinez, L. Piñuel, G.R. Castro, J.D. Breccia, Polyvinyl alcohol-pectin cryogel films for controlled release of enrofloxacin, *Appl. Biochem. Biotechnol.* 67 (2012) 1421–1429.
- [12] A. Nilasaroya, L.A. Poole-Warren, J.M. Whitelock, P.J. Martens, Structural and functional characterization of polyvinyl alcohol and heparin hydrogels, *Biomaterials* 29 (2008) 4658–4664.
- [13] A. Chhatari, J. Bajpai, A.K. Bajpai, Designing polysaccharide-based antibacterial biomaterials for wound healing applications, *Biomaterials* 1 (2011) 189–197.
- [14] O.M. Paduraru, D. Ciolacu, R.N. Darie, C. Vasile, Synthesis and characterization of polyvinyl alcohol/cellulose cryogels and their testing as carriers for a bioactive component, *Mater. Sci. Eng. C Mater. Biol. Appl.* 32 (2012) 2508–2515.
- [15] C.D. Varganici, O.M. Paduraru, L. Rosu, D. Rosu, B.C. Simionescu, Thermal stability of some cryogels based on poly(vinyl alcohol) and cellulose, *J. Anal. Appl. Pyrol.* 104 (2013) 77–83.
- [16] H. Tilly, A spectroscopic study of photoirradiated cellulose, *J. Photochem. Photobiol. A: Chem.* 76 (1993) 143–149.
- [17] C.C. Lin, L.T. Lee, L.J. Hsu, Performance of UV/S<sub>2</sub>O<sub>8</sub><sup>2-</sup> process in degrading polyvinyl alcohol in aqueous solutions, *J. Photochem. Photobiol. A: Chem.* 252 (2013) 1–7.
- [18] D. Rosu, C.-A. Teaca, R. Bodirlau, L. Rosu, FTIR and color change of the modified wood as a result of artificial light irradiation, *J. Photochem. Photobiol. B: Biol.* 149 (2010) 383–388.
- [19] A. Sionkowska, A. Planecka, J. Kozłowska, J. Skopińska-Wisniewska, Photochemical stability of poly(vinyl alcohol) in the presence of collagen, *Polym. Degrad. Stab.* 94 (2009) 383–388.
- [20] A. Sionkowska, Effects of solar radiation on collagen and chitosan films, *J. Photochem. Photobiol. B: Biol.* 82 (2006) 9–15.
- [21] H. Kaczmarek, A. Podgórski, K. Bajer, Photochemical reactions in poly(vinyl chloride)/poly(vinyl alcohol) blends, *J. Photochem. Photobiol. A: Chem.* 171 (2005) 187–195.
- [22] N. Nagai, T. Matsunobe, T. Imai, Infrared analysis of depth profiles in UV-photochemical degradation of polymers, *Polym. Degrad. Stab.* 88 (2005) 224–233.
- [23] M. Silverstein, F.S. Webster, D.J. Kiemle (Eds.), *Spectrometric Identification of Organic Compounds*, seventh ed., John Wiley & Sons, New York, 2005, pp. 83.
- [24] D.K. Banerjee, C.C. Budke, Spectrophotometric determination of traces of peroxides in organic solvents, *Anal. Chem.* 36 (1964) 792–796.
- [25] M. Yatagai, S.H. Zeronian, Effect of ultraviolet light and heat on the properties of cotton cellulose, *Cellulose* 1 (1994) 205–214.
- [26] J.L. Gardette, S. Gaumet, J. Lemaire, Photooxidation of poly(vinyl chloride). 1. A re-examination of the mechanism, *Macromolecules* 22 (1989) 2576–2581.
- [27] S. Gaumet, J.L. Gardette, Photo-oxidation of poly(vinylchloride): 2. A comparative study of thermo- and photo-oxidations, *Polym. Degrad. Stab.* 33 (1991) 17–34.
- [28] A.T. Balaban, M. Banciu, I. Pogany, *Applications of Physical Methods in Organic Chemistry*, Scientific and Encyclopedic Publisher, Bucharest, 1983.
- [29] L.J. Bellamy (Ed.), *The Infrared Spectra of Complex Molecules*, Chapman and Hall Publishers Ltd., London, 1975.
- [30] G.S. El Bahy, M. El-S. El-Sayed, A.A. Mahmoud, N.M. Gweily, Preparation and characterization of poly vinyl alcohol/gelatin blends, *J. Appl. Sci. Res.* 8 (2012) 3544–3551.

- [31] X. Colom, F. Carrillo, F. Nogues, P. Garriga, Structural analysis of photodegraded wood by means of FTIR spectroscopy, *Polym. Degrad. Stab.* 80 (2003) 543–549.
- [32] S.Y. Oh, D.I. Yoo, Y. Shin, G. Seo, FTIR analysis of cellulose treated with sodium hydroxide and carbon dioxide, *Carbohydr. Res.* 340 (2005) 417–428.
- [33] K.K. Pandey, A study of chemical structure of soft and hardwood and wood polymers by FTIR spectroscopy, *J. Appl. Polym. Sci.* 71 (1999) 1969–1975.
- [34] D. Rosu, L. Rosu, F. Mustata, C.D. Varganici, Effect of UV radiation on some semi-interpenetrating polymer networks based on polyurethane and epoxy resin, *Polym. Degrad. Stab.* 97 (2012) 1261–1269.
- [35] X. Gu, D. Stanley, W.E. Byrd, D. Dickens, I. Vaca-Trigo, W.Q. Meeker, T. Nguyen, J. W. Chin, J.W. Martin, in: J.W. Martin, R.A. Ryntz, J. Chin, R. Dickie (Eds.), *Service Life Prediction of Polymeric Materials – Global Perspectives*, Springer Science and Business Media, New York, 2009, pp. 3–28.
- [36] J. Gaume, P. Wong-Wah-Chung, A. Rivaton, A. Thérias, J.-L. Gardette, Photochemical behavior of PVA as an oxygen-barrier polymer for solar cell encapsulation, *RSC Adv.* 1 (2011) 1471–1481.
- [37] J.L. Ferreira, M.J. Melo, A.M. Ramos, Poly(vinyl acetate) paints in works of art: a photochemical approach. Part 1, *Polym. Degrad. Stab.* 95 (2010) 453–461.
- [38] S. Wei, V. Pintus, M. Schreiner, Photochemical degradation study of polyvinyl acetate paints used in artworks by Py-GC/MS, *J. Anal. Appl. Pyrol.* 97 (2012) 158–163.
- [39] K. Ma, F.R. van de Voort, J. Sedman, A.A. Ismail, Stoichiometric determination of hydroperoxides in fats and oils by Fourier transform infrared spectroscopy, *J. Am. Oil Chem. Soc.* 74 (8) (1997) 897–906.
- [40] P. Calvini, A. Gorassini, FTIR – deconvolution spectra of paper documents, *Restaurator* 23 (1) (2002) 48–66.
- [41] R.L. Desai, J.A. Shields, Photochemical degradation of cellulose material, *Macromol. Chem. Phys.* 122 (1) (1969) 134–144.
- [42] L.M. Matuana, J.J. Balatinez, R.N.S. Sodhi, C.B. Park, Surface characterization of esterified cellulosic fibers by XPS and FTIR spectroscopy, *Wood Sci. Technol.* 35 (2001) 191–201.